Integrated Control of Internal Boundary and Ramp Inflows for Lane-free Traffic of Automated Vehicles on Freeways

Xufeng Jin, Xianghua Yu, Yonghui Hu, Yibing Wang*, Markos Papageorgiou, Ioannis Papamichail, Milad Malekzadeh

***Abstract*—This paper is concerned with a novel traffic control concept of internal boundary control for bi-directional lane-free traffic of automated vehicles on freeways. The internal boundary control can help exploit the capacity resources of road infrastructure and eliminate traffic jams by sharing the total bi-directional capacity for traffic on freeways when the total demand of the bi-directional traffic (also in consideration of on/off-ramp flows in both directions) does not exceed the total capacity. When this condition is not met, however, applying the internal boundary control alone cannot reach the pursued goal. Thus, one other traffic control measure ramp metering is introduced as well. This paper studies how to prevent freeway congestion using both control measures. A cell transmission model (CTM) based non-holding-back quadratic programming optimal control model is formulated. The investigation results show that the proposed integrated control scheme can maximize the utilization of road infrastructure and remove congestion at overloaded ramp-merging areas. It is the first time to study the combination of the two control measures and its potential.**

I. Introduction

Due to the steady growth in traffic demand, traffic congestion happens increasingly frequently on freeways, especially during holidays, morning and evening peek-periods, which causes a series of problems such as travel delays, traveler injuries, environmental pollution. In the past few decades, ramp metering, variable speed limit control and other freeway traffic control measures have been applied to improve traffic conditions [1], [2]. However, all those measures face various limitations. The emergence of connected and automated vehicles (CAVs) critically helps to tackle the limitations, and opens a new era of freeway traffic control [3].

Based on automated driving, vehicle-to-vehicle (V2V), vehicle-to-infrastructure (V2I) communication and other related technologies, a novel paradigm of vehicular traffic "*TrafficFluid*" that is applicable at high penetration rates of CAVs, was proposed recently [4]. *TrafficFluid* has the following features: (1) lane-free traffic: directional vehicles are no longer restricted by fixed traffic lanes, but only bound to the road boundaries, and can drive anywhere within the boundaries. (2) nudging: vehicles can communicate their status and plans with others and particularly exert a pushing force towards vehicles in front, which is impossible for human-driven vehicular traffic where anisotropy is dominating [4]. Based on the two principles, vehicles will not form lanes, but 2-D clusters on roads. The microscopic simulation results in [4] show that, as long as the two principles were applied, the resulting road capacity would be enlarged drastically.

In this context, a new concept of traffic control called internal boundary control was proposed [5]. it exploits and extends the lane-free feature of *TrafficFluid* to consider that the internal boundary between the two opposite directions of traffic on a road is not necessarily fixed but can be flexible under the lane-free paradigm of CAV traffic. As such, the total bi-directional cross-road capacity can be shared between the two directions according to their respective demands to maximize road space utilization. Internal boundary control can be achieved by setting a virtual internal boundary between the two opposite traffic flows and sending this information to CAVs in order for them to be aware of this boundary while performing their lane-free-based maneuvers. With appropriate control strategies, the internal boundary can be adjusted in adequate resolutions of time and space for the optimization of traffic efficiency.

The concept of sharing capacity can be traced back to reversible lanes, which has been successfully implemented in many freeways, e.g. Interstate 15 in San Diego, Canal Road in Washington [6] to address a variety of needs, e.g. unbalanced peek-period traffic demands [7], special event management [8]. Some other works (e.g. [13]) modified the types of usage (e.g. through, turning) of one or more lanes to reallocate the available road resources to meet unbalanced and varying traffic demands. Early works as mentioned above were usually done offline based on experience to manually modify the corresponding lane boundaries using e.g. traffic signs or roadblocks.

To make the operation more efficient, a number of subsequent works have tried to establish control strategies so as to adjust reversible lanes in real time according to traffic conditions. To this end, some approaches have been employed, such as binary mixed-integer linear programming [9], multi-objective mixed-integer non-linear programming [10], feedback control [11], model predictive control (MPC) [12]. However, those models did not take advantages of the real-time traffic information available with CAV technologies, except that Ding [13] constructed a mixed integer quadratic programming to jointly optimize signal timings and variable lane settings in a CAV environment.

X.Jin, X.Yu, Y.Hu, and Y.Wang are with the Institute of Intelligent Transportation Systems, Zhejiang University, 310058 Hangzhou, China (e-mail: wangyibing@zju.edu.cn)

M.Papageorgiou, I.Papamichail, and M.Malekzadeh are with the Dynamic Systems and Simulation Laboratory, Technical University of Crete, 73100 Chania, Greece (e-mail: markos@dssl.tuc.gr)

The above lane-based tidal flow control systems have obvious shortcomings and limitations [5]. More specifically, (1) The spatial resolution for lane operation is very restrictive, which is lane based and not sufficient for tricky but not rare situations under which the demand difference in the two opposite directions may not be more than the capacity of one lane, and if possible, finer operations based on a portion of a lane would be ideal. (2) For safety, the clearance time of the reversible lane after each lane switch is long, wasting space resources. (3) The reversible lane must be long enough to avoid congestion in the interleaved lane. By contrast, in the TrafficFluid environment, these problems can readily be handled, thanks to the characteristics of lane-free traffic and nudging operations. The internal boundary control in this environment can achieve the sharing of capacity with a high lateral resolution of reversible lanes, short control interval and short road length.

Recently, Malekzadeh [5] analyzed the performance of internal boundary control for freeways based on convex quadratic programming. The work has a high potential for further improvements. Malekzadeh [14] also applied Linear-Quadratic regulators to the problem of internal boundary control, enabling efficient real-time capacity sharing without traffic demand prediction. However, both works only verified the concept of internal boundary control under simple traffic scenarios. When the condition gets more complex, it may not be sufficient to eliminate congestion. For instance, when the sum of bi-directional demands is greater than the total capacity of all lanes in two directions, especially considering on-ramp inflows, congestion cannot be avoided by applying internal boundary control alone.

With the above in mind, and also to fully explore the potential of internal boundary control, a more general control problem is studied in this paper, which combines the internal boundary control with ramp metering. By handling this problem under critically congested traffic conditions, the applicable scenarios, limitations and the pros and cons of internal boundary control can be examined in depth, and the gained knowledge could be valuable for a general internal boundary control model in the CAV environment.

More specifically, this paper formulates a CTM-model-based optimization scheme for an integrated problem of internal boundary control and ramp metering on freeways. It analyzes and elaborates on the characteristics of the problem. In particular, a convex quadratic programming (QP) problem is treated to avoid the holding-back issue [15] so as to obtain reasonable results. Finally, the scheme is tested in a carefully designed freeway scenario with satisfactory results obtained.

The contributions of this work are as follows: (1) It is for the first time to combine the internal boundary control and ramp metering for freeway traffic and study the compatibility of the two control measures and their potential in improving traffic flow efficiency. (2) In the lane-free paradigm of CAVs, it is possible to order via internal boundary control all road resources including ramp storage space in both directions to work together for traffic flow optimization, which is absolutely impossible in the current traffic paradigm with fixed internal boundaries. It is for the first time to study this novel possibility.

The remainder of the paper is organized as follows: Section II presents the idea of internal boundary control and the corresponding mathematical model. CTM and the optimal control framework are given in Section III. Section IV introduces the formulation of the quadratic programming. Case study and corresponding results are presented in Section V. Section VI concludes this paper.

II. Internal Boundary Modeling

In the TrafficFluid environment, the structure of the existing macroscopic models will not be changed, in contrast, some concepts like the conservation equation, the fundamental diagram and the moving traffic waves will continue to characterize macroscopic traffic flow modeling [5]. The only differences are the free speed, critical density, flow capacity. These values may differ from in lane-based traffic and when the internal boundary control comes into play, these values will no longer be constant, but change dynamically.

Hence, before establishing the macroscopic dynamic traffic model for internal boundary control and ramp metering, it is crucial to analyze the characteristics of the two opposite traffic directions with the impact of internal boundary control. As explicitly derived in[4], [5], for the scene show in Figure 1. , the relationship between key parameters of the respective Fundamental Diagrams (FDs) such as Q_{cap}^{a}, Q_{cap}^{b}, ρ_{cr}^{a}, ρ_{cr}^{b} and the sharing factor ε is linear. The specific derivation is as follows.

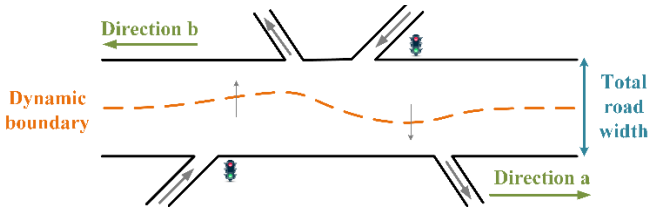

Figure 1. Space-time internal road boundary

As is shown in Figure 1. , there are two opposite traffic directions, which we will call direction a and direction b. The road widths of direction a and direction b are $w^a = \varepsilon \cdot w$ and $w^b = (1-\varepsilon) \cdot w$, where w is the total road width and $0 \leq \varepsilon \leq 1$ is the sharing factors. The total FD of the highway segment is Q(ρ), where ρ is the traffic density in veh/km. Assuming w is the total number of lanes and $\varepsilon \cdot w$, $(1-\varepsilon) \cdot w$ are the corresponding integer numbers of lanes for the two directions. The FD per lane can be easily get as $Q(\rho^1 \cdot w)/w$ where ρ^1 is the density per lane and similarly, the FDs for the two directions, are given in the form of ε's functions.

$$Q^a(\rho^a, \varepsilon) = \varepsilon \cdot Q(\rho^a / \varepsilon) \tag{1}$$

$$Q^b(\rho^b, \varepsilon) = (1-\varepsilon) \cdot Q(\rho^b / (1-\varepsilon)) \tag{2}$$

in which ρ^a and ρ^b are the respective densities of the two directions.

As for direction a, by taking the derivative of (1), we can obtain that $Q^{a\prime}(\rho^a, \varepsilon) = Q'(\rho^a/\varepsilon)$. For the critical density ρ_{cr}^a, we have $Q^{a\prime}(\rho_{cr}^a, \varepsilon) = 0 = Q'(\rho_{cr}^a/\varepsilon)$. Meanwhile, we also have $Q'(\rho_{cr}) = 0$. Hence, it can be easily deduced that $\rho_{cr}^a(\varepsilon) = \varepsilon \cdot \rho_{cr}$. For the capacity, we have $q_{cap}^a = Q^a(\rho_{cr}^a, \varepsilon) = \varepsilon \cdot Q(\rho_{cr}) = \varepsilon \cdot q_{cap}$. As for the jam density, we

have $Q(\rho_{max}) = Q^a(\varepsilon \cdot \rho_{max}, \varepsilon) = 0$ and deduce that $\rho^a_{max}(\varepsilon) = \varepsilon \cdot \rho_{max}$.

Similarly, we can deduce $\rho^b_{cr}(\varepsilon) = (1-\varepsilon)\,\rho_{cr}$, $q^b_{cap}(\varepsilon) = (1-\varepsilon) q_{cap}$ and $\rho^b_{max}(\varepsilon) = (1-\varepsilon) \cdot \rho_{max}$ for direction *b*.

III. CTM-BASED OPTIMAL CONTROL

A. General Framework

In this work, we consider exploring the potential of combining internal boundary control and ramp metering in congested freeway environment. A general macroscopic traffic model for internal boundary control and ramp metering is expressed as follows:

$$x^a(k+1) = f^a[x^a(k), \varepsilon^a(k_c), r^a(k_r), t^a(k)] \tag{3}$$

$$x^b(k+1) = f^b[x^b(k), \varepsilon^b(k_c), r^b(k_r), t^b(k)] \tag{4}$$

where x^a and x^b are the state vectors for traffic directions *a* and *b*; k = 0,1, ... is the corresponding discrete time index; $t^a(k)$ and $t^b(k)$ are vectors of external variables in the respective traffic directions *a* and *b* (upstream demand, initial density etc.); ε^a and ε^b are the vectors of the corresponding sharing factors; r^a and r^b are the vectors of ramp metering flow. The internal boundary control time step T_c is assumed to be a multiple of the model time step T, hence the control time index is given by $k_c = \lfloor kT/T_c \rfloor$, in which $\lfloor\ \rfloor$ means to take the integer part. Same as the ramp metering time step T_r and time index k_r.

By the way, the relationship between $\varepsilon(k_c)$, $\varepsilon^a(k_c)$ and $\varepsilon^b(k_c)$ should be emphasized. For traffic safety, the time-delay should apply only to the traffic direction that is being widened, while the direction that is restricted should promptly apply the smaller width. The purpose of $\varepsilon^a(k_c)$ and $\varepsilon^b(k_c)$ is to achieve this time-delay by establishing the mathematical relationship with $\varepsilon(k_c)$. The relationship can be expressed as follows:

$$\varepsilon^a_i(k_c) = \min\{\varepsilon_i(k_c), \varepsilon_i(k_c - 1)\} \tag{5}$$

$$\varepsilon^b_i(k_c) = \min\{1-\varepsilon_i(k_c), 1-\varepsilon_i(k_c - 1)\} \tag{6}$$

What's more, the sharing factor ε_i should be constrained to prevent the complete closure of the road in either direction but assign the road width in either direction will be bigger than the widest vehicles. The constraint is shown in (7)

$$0 < \varepsilon_{i,min} \le \varepsilon_i \le \varepsilon_{i,max} < 1 \tag{7}$$

where $\varepsilon_{i,min} \cdot w$ and $(1-\varepsilon_{i,max}) \cdot w$ are the minimum widths to be assigned in either direction.

B. CTM model

Cell Transmission Model (CTM) [16] is a first-order model deriving from the LWR model. Because of its triangular FD, it can form a convex, linear or quadratic programming problem easily and solved quickly when used in an optimization problem. In this work, we select the extended CTM model which can reproduce the capacity drop [17] and modify it to achieve internal boundary control.

Before present the CTM equations, let us first introduce the key notations corresponding with Figure 2. . The highway stretch we consider, has n segments, with respective lengths L_i.For direction *a*, traffic flows from segment 1 to segment n. The $\rho^a_i, i = 1,2,\dots,n$ are the traffic density of segment *i*, and $q^a_i, i = 1,2,\dots,n$ are the mainstream exit flows of segment *i*. For on-ramps may exist in some segments, we denote $r^a_i, i = 1,2,\dots,n$, the on-ramp flow for segment *i*, and $w^a_i, i = 1,2,\dots,n$, the ramp queues for segment *i*. For off-ramps, we have exit rates β^a_i, and the exit flow of segment *i* can be calculated as $\beta^a_i \cdot q^a_i$ Similarly, for direction *b*, we denote the traffic density $\rho^b_i, i = 1,2,\dots,n$, the mainstream exit flow $q^b_i, i = 1,2,\dots,n$, on-ramp flow $r^a_i, i = 1,2,\dots,n$, the ramp queues $w^a_i, i = 1,2,\dots,n$, and the off-ramp exit rates β^b_i.

Based on these definitions, the conservation of each segment can be written for direction *a* and direction *b* respectively:

$$\rho^a_i(k+1) = \rho^a_i(k) + \frac{T}{L_i}((1-\beta^a_i) q^a_{i-1}(k) - q^a_i(k) + r^a_i(k_r)),$$
$$i = 1,2,\dots,n \tag{8}$$

$$\rho^b_i(k+1) = \rho^b_i(k) + \frac{T}{L_i}((1-\beta^b_i) q^b_{i+1}(k) - q^b_i(k) + r^b_i(k_r)),$$
$$i = 1,2,\dots,n \tag{9}$$

where the $q^a_i(k)$ and $q^b_i(k)$ are obtained by upstream demand and downstream supply according to the following equations:

$$q^a_i(k) = \min\{Q_D(\rho^a_i(k), \varepsilon^a_i(k_c)), \frac{Q_S(\rho^a_{i+1}(k), \varepsilon^a_{i+1}(k_c)}{1-\beta^a_{i+1}}$$
$$-\lambda_r r^a_{i+1}(k)\}, i = 1,2,\dots,n-1,$$
$$q^a_n(k) = Q_D(\rho^a_i(k), \varepsilon^a_i(k_c)) \tag{10}$$

$$q^b_i(k) = \min\{Q_D(\rho^b_i(k), \varepsilon^b_i(k_c)), \frac{Q_S(\rho^b_{i-1}(k), \varepsilon^b_{i-1}(k_c)}{1-\beta^b_{i-1}}$$
$$-\lambda_r r^b_{i-1}(k)\}, i = 2,3,\dots,n,$$
$$q^b_n(k) = Q_D(\rho^b_i(k), \varepsilon^b_i(k_c)) \tag{11}$$

the demand function Q_D and the supply function Q_S are given by the following equations respectively:

$$Q_D(\rho, \varepsilon) = \min\{\varepsilon q_{cap} + \lambda_d q_{cap} \frac{\rho - \varepsilon\rho_{cr}}{\rho_{cr} - \rho_{\max}}, v_f \rho\} \tag{12}$$

$$Q_S(\rho, \varepsilon) = \min\{\varepsilon q_{cap}, w_s(\varepsilon\rho_{\max} - \rho)\} \tag{13}$$

where v_f is the free speed, w_s is the back-wave speed, λ_d and λ_r are the parameters to activate capacity drop [17].

What's more, the ramp queues are determined by the followings:

$$w^a_i(k+1) = w^a_i(k) + T[d^a_i(k) - r^a_i(k_r)]$$
$$w^b_i(k+1) = w^b_i(k) + T[d^b_i(k) - r^b_i(k_r)] \tag{14}$$

where $d^a_i(k)$, $d^b_i(k)$ are the on-ramp demand.

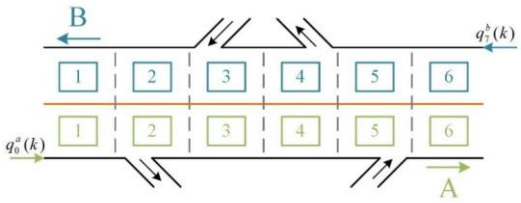

Figure 2. The considered highway stretch

IV. QUADRATIC PROGRAMMING FORMULATION

To complete the QP problem formulation, the non-linear equations should be linearized. The non-linear CTM equations (10,11) can yield the following linear inequalities:

For direction *a* (equation (10)):

$$q_i^a(k) \le v_f \rho_i^a(k), i = 1,2,...n \tag{15}$$

$$q_i^a(k) \le \varepsilon_i^a(k_c) q_{cap} + \lambda_d q_{cap} \frac{\rho_i^a(k) - \varepsilon_i^a(k_c)\rho_{cr}(k_c)}{\rho_{cr} - \rho_{\max}}, \tag{16}$$
$$i = 1,2,\dots n$$

$$q_i^a(k) \le \frac{w_s}{(1-\beta_{i+1}^a)}(\varepsilon_{i+1}^a(k_c)\rho_{\max} - \rho_{i+1}^a(k)) - \lambda_r r_{i+1}^a(k_r), \tag{17}$$
$$i = 1,2,\dots n-1$$

$$q_i^a(k) \le \frac{\varepsilon_{i+1}^a(k_c) q_{cap}}{(1-\beta_{i+1}^a)} - \lambda_r r_{i+1}^a(k_r), i = 1,2,\dots n-1 \tag{18}$$

For direction *b* (equation (11)):

$$q_i^b(k) \le v_f \rho_i^b(k), i = 1,2,...n \tag{19}$$

$$q_i^b(k) \le \varepsilon_i^b(k_c) q_{cap} + \lambda_d q_{cap} \frac{\rho_i^b(k) - \varepsilon_i^b(k_c)\rho_{cr}(k_c)}{\rho_{cr} - \rho_{\max}}, \tag{20}$$
$$i = 1,2,\dots n$$

$$q_i^b(k) \le \frac{w_s}{(1-\beta_{i-1}^b)}(\varepsilon_{i-1}^b(k_c)\rho_{\max} - \rho_{i-1}^b(k)) - \lambda_r r_{i-1}^b(k_r), \tag{21}$$
$$i = 2,3,\dots n$$

$$q_i^b(k) \le \frac{\varepsilon_{i-1}^b(k_c) q_{cap}}{(1-\beta_{i-1}^b)} - \lambda_r r_{i-1}^b(k_r), i = 2,3,\dots n \tag{22}$$

Similarly, the equation (5), (6) can be modified into the following inequations:

$$\varepsilon_i^a(k_c) \le \varepsilon_i(k_c) \tag{23}$$

$$\varepsilon_i^a(k_c) \le \varepsilon_i(k_c - 1) \tag{24}$$

$$\varepsilon_i^b(k_c) \le 1 - \varepsilon_i(k_c) \tag{25}$$

$$\varepsilon_i^b(k_c) \le 1 - \varepsilon_i(k_c - 1) \tag{26}$$

Hence, the linear inequalities of the QP derive from all inequalities include (15)-(26), while (8), (9), (14) are the linear equality. The decision variables include all the state ($\rho_i^a(k), \rho_i^b(k), q_i^a(k), q_i^b(k), w_i^b(k), w_i^b(k)$) and control variables ($\varepsilon_i(k_c), \varepsilon_i^a(k_c), \varepsilon_i^b(k_c), \varepsilon_i^b(k_c), r_i^a(k_r), r_i^b(k_r)$).

The cost criterion, which consider the control goal and the system robustness, is defined as (27). The cost criterion includes nine terms. The first two terms present the Total Time Spent (TTS), which is one of the most important parameters to evaluate traffic flow efficiency. The third (weighted by w_1) and fourth terms (weighted by w_2) are one of the major innovations, in which h_i obey the rule that $h_i > h_j > 0, \forall i,j \epsilon n, i < j$, and g_i obey the rule that $0 < g_i < g_j, \forall i,j \epsilon n, i < j$. By setting appropriate parameters, they can overcome the holding-back phenomenon [15], which is a non-physical phenomenon caused by the linearization of nonlinear equations. The fifth term aims to maximize road resource utilization, and the next three terms are penalty terms for minimizing the variation of the control input in time and space. The last term is policy related, which is considered to balance the respective capacity reserves for each segment. More detailed explanation can be seen in [5].

$$\begin{aligned} J = {} & T\sum_{k=1}^{K}\sum_{i=1}^{n}\left(L_i\rho_i^a(k) + L_i\rho_i^b(k)\right) + T\sum_{k=0}^{K}\sum_{i=1}^{n}\left(w_i^a(k) + w_i^b(k)\right) \\ & - w_1\left[\sum_{k=1}^{K}\sum_{i=1}^{n}\left(Q_i^a(k) + Q_i^b(k)\right) + \sum_{k=1}^{K_r}\sum_{i=1}^{n}\left(r_i^a(k_r) + r_i^b(k_r)\right)\right] \\ & + w_2\sum_{k=1}^{K-1}\sum_{i=1}^{n}\left(h_i \cdot \rho_i^a(k) + g_i \cdot \rho_i^b(k)\right) \\ & - w_3\sum_{k_c=0}^{K_c-1}\sum_{i=1}^{n}\left(\varepsilon_i^a(k_c) + \varepsilon_i^b(k_c)\right) + w_4\sum_{k_r=1}^{K_r}\sum_{i=1}^{n}[r_i^{dir}(k_r) - r_i^{dir}(k_r - 1)]^2 \\ & + w_5\sum_{k_c=1}^{K_c-1}\sum_{i=1}^{n}\left(\varepsilon_i(k_c) - \varepsilon_i(k_c - 1)\right)^2 + w_6\sum_{k_c=0}^{K_c-1}\sum_{i=2}^{n}\left(\varepsilon_i(k_c) - \varepsilon_{i-1}(k_c)\right)^2 \\ & + w_7\sum_{k_c=0}^{K_c-1}\sum_{i=1}^{n}\left(\frac{\varepsilon_i(k_c)^2}{d_i^a(k_c)} + \frac{(1-\varepsilon_i(k_c))^2}{d_i^b(k_c)}\right) \end{aligned} \tag{27}$$

V. SIMULATION

The selected highway stretch, same as in [5], is displayed in Figure 2. . It is 3 km long and evenly divided into six segments. In direction *a*, there is one on-ramp at segment 5 and one off-ramp at segment 2. In direction *b*, there is one on-ramp at segment 3 and one off-ramp at segment 4. All the on-ramps and the off-ramps are located at the beginning of the corresponding segments.

The modelling time step is $T = 10s$, the internal boundary control time step is $T_c = 60s$ and the ramp metering time step is $T_r = 60s$. The considered time horizon is 1 hour, hence, $K = 360$, $K_c = 60$, $K_r = 60$. The CTM corresponding parameters are $V_f = 100km/h$, $w_s = 12km/h$, $q_{cap} = 12000veh/h$, $\rho_{cr} = 120veh/km$, $\rho_{max} = 1120veh/km$. The parameters to activate capacity drop, are $\lambda_d = 0.4, \lambda_r = 0.7$. The upper and lower bounds for the sharing factors ε is $\varepsilon_{min} = 0.16, \varepsilon_{max} = 0.84$, respectively. For all the segments, the initial density values are $\rho_i(0) = 5veh/km$ and for all the off-ramps, the exiting rates are 0.1.

The demand flows are shown in Figure 3. . For both directions, the distribution of mainstream demand is similar. They have the same peak value, and the peaks are greatly overlapping. Meanwhile, the on-ramp demands in both directions are constant, and the on-ramp demand in direction *a*

is higher than in direction *b*. The traffic demand scenario can activate the state that the total demand of the bi-directional traffic exceed the total capacity and is suitable for validating the proposed model.

The weight parameters in the cost criterion are obtained by gradually increased when the value of TTS increases marginally but the corresponding issues, e.g. holding-back, smoothness are achieved at a sufficient level. More precisely, $w_1 = 10^{-4}$, $w_2 = 10^{-3}$, $w_3 = 10^{-5}$, $w_4 = 10^{-4}$, $w_5 = 10^{-6}$, $w_6 = 10^{-6}$, $w_7 = 10^{-5}$.

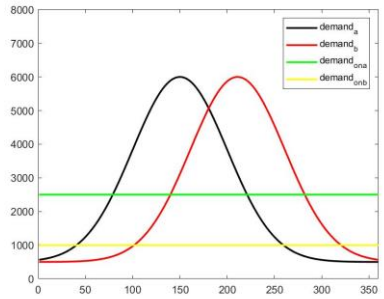

Figure 3. Traffic demand for all the directions and on-ramps

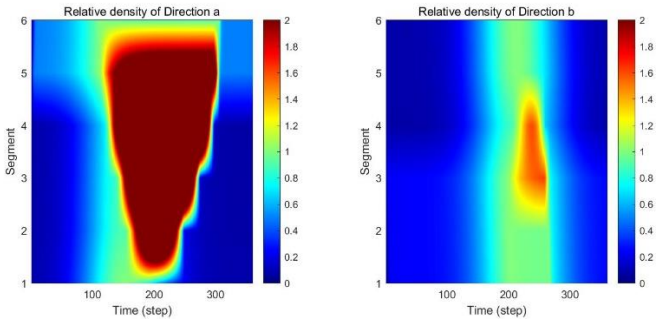

Figure 4. Spatio-temporal relative density in the no-control case

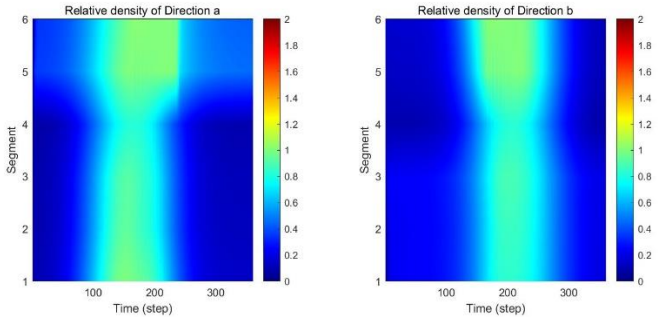

Figure 5. Spatio-temporal relative density in the control case

For comparison, the simulation results of the no-control case are shown first in Figure 4. . In this case, the sharing factors are constant of $\varepsilon_i = 0.5$ for all segments, and all the on-ramp flows will enter the mainstream without control. In the no-control case, the value of TTS for the scenario is 310.6 veh · h and the value of Total Delay (TD) is 137.0 veh · h. Figure 4. displays the corresponding spatio-temporal density evolution. The variable displayed in Fig.4 is the relative density, which is defined as $\rho^{\sim a}(k) = \rho^a(k)/\varepsilon^a(k) \cdot \rho_{cr}$, $\rho^{\sim b}(k) = \rho^b(k)/\varepsilon^b(k) \cdot \rho_{cr}$, same as the spatio-temporal density figure in the following control case. According to the definition, the value of relative density lower than 1 refer to uncongested traffic, and value higher than 1 refer to congested traffic. Figure 4. shows that there is a heavy congestion in segment 5 for direction *a*, which occurs at around k = 110 for the increased mainstream demand. The congestion spread upstream to segment 2 and dissolve at around k = 280. In direction *b*, a congestion occurs at around k = 210 in segment 3, spills back up to segment 4 and dissolves at around k = 270. The congestion in direction *b* is smaller than in direction a for the lower on-ramp demand.

The simulation results of the control case are displayed in Figure 5. . We can briefly see that the proposed optimal control model can eliminate the congestion by capacity sharing and ramp metering. It needs to be emphasized that there is no holding-back phenomenon in the simulation results, which means that only the proposed control methods have an impact on the traffic flow.

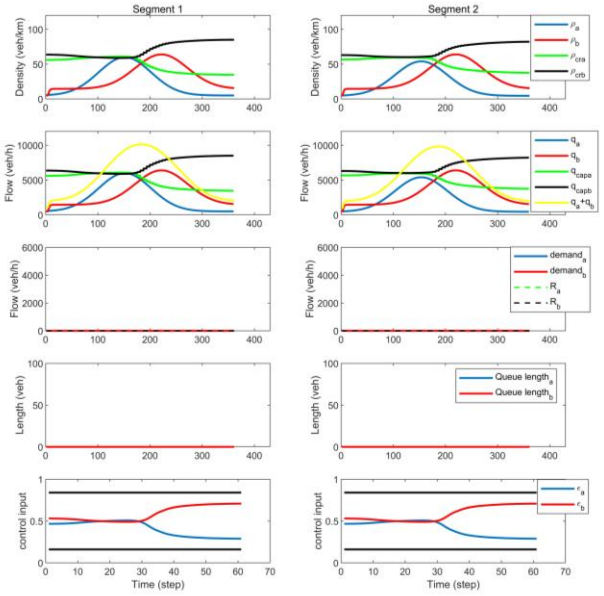

Figure 6. Density, flow and control trajectories for segment 1 and 2

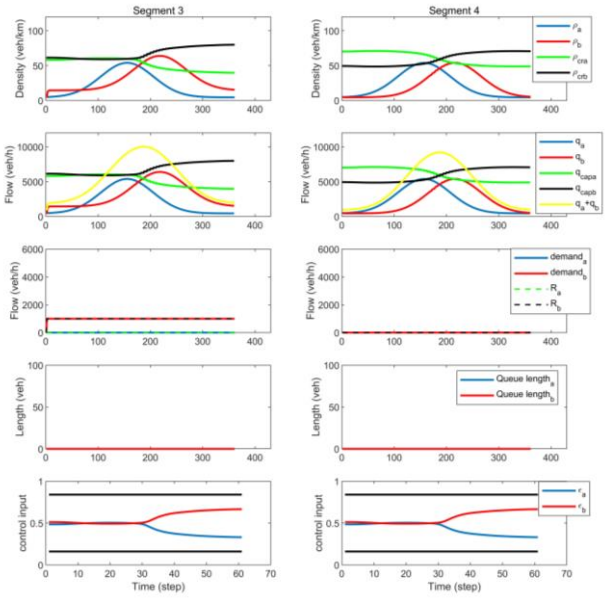

Figure 7. Density, flow and control trajectories for segment 3 and 4

More information can be seen in Figure 6. , 7, 8. For each segment, five diagrams are presented. The first one shows the two traffic densities and the corresponding critical densities. Flows and capacity are shown in the second one. The third one provides the ramp metering flow and on-ramp demand for each segment, and the forth one shows the ramp queue length. The last one presents the trajectories of the sharing factors, in which the black lines mean the upper and lower boundaries for the sharing factors.

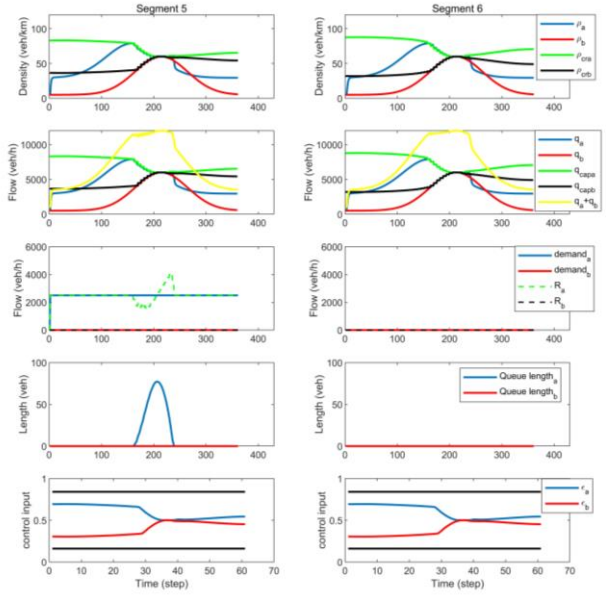

Figure 8. Density, flow and control trajectories for segment 5 and 6

The results show that the densities (flows) are always lower than the critical densities (capacities) in all segments. The proposed controller assigns new capacities for both directions according to their demands during the whole horizon, which can help avoid congestion. The ramp metering comes into play when the demand in direction *a* arrive its peak at around $k = 180$, meanwhile more capacity is assigned to direction *a*. By the help of internal boundary control and ramp metering, the total flow curve reach the total capacity during the heavy congestion period. In short, the congestion is utterly avoided while the utilization of road infrastructure is maximized. The value of TTS is 183.3 veh · h, which is 41.0% less than TTS in no-control case. TD has more noticeable improvements. The simulation resulting TD value is equal to 9.7 veh · h, that is an improvement of 92.9% over the no-control case.

VI. Conclusion

Integrated control of internal boundary and ramp inflows for lane-free traffic of automated vehicles on freeways has been studied in this paper. A CTM-based quadratic programming optimal control model has been employed to design the integrated controller for both internal boundary control and ramp metering, with particular attention given to the holding-back issue. The study results demonstrate that the proposed integrated control scheme can make up for the deficiency of internal boundary control alone and has the potential of avoiding congestion, maximizing the utilization of road infrastructure and improving the traffic flow efficiency.

References

[1] Y. Wang *et al.*, "Freeway Traffic Control in Presence of Capacity Drop," *IEEE Trans. Intell. Transport. Syst.*, vol. 22, no. 3, pp. 1497–1516, Mar. 2021, doi: 10.1109/TITS.2020.2971663.

[2] M. Papageorgiou, C. Kiakaki, V. Dinopoulou, A. Kotsialos, and Yibing Wang, "Review of road traffic control strategies," *Proc. IEEE*, vol. 91, no. 12, pp. 2043–2067, Dec. 2003, doi: 10.1109/JPROC.2003.819610.

[3] C. Diakaki, M. Papageorgiou, I. Papamichail, and I. Nikolos, "Overview and analysis of Vehicle Automation and Communication Systems from a motorway traffic management perspective," *Transportation Research Part A: Policy and Practice*, vol. 75, pp. 147–165, May 2015, doi: 10.1016/j.tra.2015.03.015.

[4] M. Papageorgiou, K.-S. Mountakis, I. Karafyllis, I. Papamichail, and Y. Wang, "Lane-Free Artificial-Fluid Concept for Vehicular Traffic," *Proc. IEEE*, vol. 109, no. 2, pp. 114–121, Feb. 2021, doi: 10.1109/JPROC.2020.3042681.

[5] M. Malekzadeh, I. Papamichail, M. Papageorgiou, and K. Bogenberger, "Optimal internal boundary control of lane-free automated vehicle traffic," *Transportation Research Part C: Emerging Technologies*, vol. 126, p. 103060, May 2021, doi: 10.1016/j.trc.2021.103060.

[6] B. Wolshon and L. Lambert, "Reversible Lane Systems: Synthesis of Practice," *J. Transp. Eng.*, vol. 132, no. 12, pp. 933–944, Dec. 2006, doi: 10.1061/(ASCE)0733-947X(2006)132:12(933).

[7] Transportation Research Board and National Academies of Sciences, Engineering, and Medicine, *Convertible Roadways and Lanes*. Washington, D.C.: Transportation Research Board, 2004, p. 23331. doi: 10.17226/23331.

[8] J. Wojtowicz and W. A. Wallace, "Traffic Management for Planned Special Events Using Traffic Microsimulation Modeling and Tabletop Exercises," *Journal of Transportation Safety & Security*, vol. 2, no. 2, pp. 102–121, Jun. 2010, doi: 10.1080/19439962.2010.487635.

[9] J. Zhao, Y. Liu, and X. Yang, "Operation of signalized diamond interchanges with frontage roads using dynamic reversible lane control," *Transp. Res. Pt. C-Emerg. Technol.*, vol. 51, pp. 196–209, Feb. 2015, doi: 10.1016/j.trc.2014.11.010.

[10] J. Zhao, W. Ma, Y. Liu, and X. Yang, "Integrated design and operation of urban arterials with reversible lanes," *Transportmetrica B: Transport Dynamics*, vol. 2, no. 2, pp. 130–150, May 2014, doi: 10.1080/21680566.2014.908751.

[11] D. Xue and Z. Dong, "An intelligent contraflow control method for real-time optimal traffic scheduling using artificial neural network, fuzzy pattern recognition, and optimization," *IEEE Trans. Contr. Syst. Technol.*, vol. 8, no. 1, pp. 183–191, Jan. 2000, doi: 10.1109/87.817703.

[12] K. Ampountolas, J. A. dos Santos, and R. C. Carlson, "Motorway Tidal Flow Lane Control," *IEEE Trans. Intell. Transport. Syst.*, vol. 21, no. 4, pp. 1687–1696, Apr. 2020, doi: 10.1109/TITS.2019.2945910.

[13] C. Ding, R. Dai, Y. Fan, Z. Zhang, and X. Wu, "Collaborative control of traffic signal and variable guiding lane for isolated intersection under connected and automated vehicle environment," *Computer-Aided Civil and Infrastructure Engineering*, p. mice.12780, Oct. 2021, doi: 10.1111/mice.12780.

[14] M. Malekzadeh, I. Papamichail, and M. Papageorgiou, "Linear-Quadratic regulators for internal boundary control of lane-free automated vehicle traffic," *Control Eng. Practice*, vol. 115, p. 104912, Oct. 2021, doi: 10.1016/j.conengprac.2021.104912.

[15] F. Zhu and S. V. Ukkusuri, "A cell based dynamic system optimum model with non-holding back flows," *Transportation Research Part C: Emerging Technologies*, vol. 36, pp. 367–380, Nov. 2013, doi: 10.1016/j.trc.2013.09.003.

[16] C. F. Daganzo, "The cell transmission model: A dynamic representation of highway traffic consistent with the hydrodynamic theory," *Transportation Research Part B: Methodological*, vol. 28, no. 4, pp. 269–287, Aug. 1994, doi: 10.1016/0191-2615(94)90002-7.

[17] M. Kontorinaki, A. Spiliopoulou, C. Roncoli, and M. Papageorgiou, "First-order traffic flow models incorporating capacity drop: Overview and real-data validation," *Transportation Research Part B: Methodological*, vol. 106, pp. 52–75, Dec. 2017, doi: 10.1016/j.trb.2017.10.014.